ELSEVIER

RESEARCH: Review

Perovskite solar cells: an emerging photovoltaic technology

Nam-Gyu Park

School of Chemical Engineering and Department of Energy Science, Sungkyunkwan University (SKKU), Suwon 440-746, Republic of Korea

Perovskite solar cells based on organometal halides represent an emerging photovoltaic technology. Perovskite solar cells stem from dye-sensitized solar cells. In a liquid-based dye-sensitized solar cell structure, the adsorption of methylammonium lead halide perovskite on a nanocrystalline TiO_2 surface produces a photocurrent with a power conversion efficiency (PCE) of around 3–4%, as first discovered in 2009. The PCE was doubled after 2 years by optimizing the perovskite coating conditions. However, the liquid-based perovskite solar cell receives little attention because of its stability issues, including instant dissolution of the perovskite in a liquid electrolyte. A long-term, stable, and high efficiency (~10%) perovskite solar cell was developed in 2012 by substituting the solid hole conductor with a liquid electrolyte. Efficiencies have quickly risen to 18% in just 2 years. Since PCE values over 20% are realistically anticipated with the use of cheap organometal halide perovskite materials, perovskite solar cells are a promising photovoltaic technology. In this review, the opto-electronic properties of perovskite materials and recent progresses in perovskite solar cells are described. In addition, comments on the issues to current and future challenges are mentioned.

Perovskite, named after the Russian mineralogist L.A. Perovski, has a specific crystal structure with the ABX_3 formula (X = oxygen, halogen). The larger A cation occupies a cubo-octahedral site shared with twelve X anions while the smaller B cation is stabilized in an octahedral site shared with six X anions. The most studied perovskites are oxides due to their electrical properties of ferroelectricity or superconductivity. Halide perovskites received little attention until layered organometal halide perovskites were reported to exhibit a semiconductor-to-metal transition with increasing dimensionality [1]. In addition to changes in electrical properties, the band gap decreased with increased dimensionality from 2D to 3D. A narrow band gap is beneficial for solar cell applications. Miyasaka et al. [2] applied 3D perovskite $CH_3NH_3PbX_3$ (X = Br, I) as an inorganic sensitizer in dye-sensitized solar cells in 2009. They demonstrated a power conversion efficiency (PCE) of 3.1% for X = Br and 3.8% for X = I. Park et al. [3] reported PCE of 6.5% using $CH_3NH_3PbI_3$. At the given TiO_2 film thickness of about 3.6 μm, $CH_3MH_3PbI_3$ perovskite showed an absorption coefficient that was 10 times greater than that of the conventional ruthenium-based molecular dye. Since organolead halide perovskite is an ionic crystal, it easily dissolves in a polar solvent. Thus, organolead halide perovskite is not suitable for liquid electrolyte-based sensitized solar cells because of stability concerns. This instability problem was solved by substituting a solid hole conductor for the liquid electrolyte. Park et al. first reported long-term stable perovskite solar cells with PCE as high as 9.7% [4]. A non-sensitization type perovskite solar cell was proposed by Snaith et al. [5] in which the mixed halide perovskite $CH_3NH_3PbI_{3-x}Cl_x$-coated Al_2O_3 film demonstrated PCE of 10.9%. Rapid progress was made over the year, and PCEs exceeding 15% were achieved using organolead halide perovskite [6,7]. Perovskite solar cell technology was selected as one of the biggest scientific breakthroughs of 2013 by the editors of *Science* and *Nature* [8,9]. This paper reviews recent progress in perovskite solar cells and examines their future.

Base technology for perovskite solar cells

The base technology for perovskite solar cells is solid-state sensitized solar cells that are based on dye-sensitized Gratzel solar cells. In 1991, O'Regan and Gratzel developed a low-cost

E-mail address: npark@skku.edu.

1369-7021/ http://dx.doi.org/10.1016/j.mattod.2014.07.007

Please cite this article in press as: N.G. Park, Mater. Today (2014), http://dx.doi.org/10.1016/j.mattod.2014.07.007

photoelectrochemical solar cell based on high surface area nanocrystalline TiO_2 film sensitized with molecular dye [10]. Although the PCE of dye-sensitized solar cells was over 12% [11], issues such as electrolyte usage raised concerns over leakage. This concern was solved by substituting a solid hole conductor for the liquid electrolyte without changing the basic concept of dye-sensitized solar cells [12]. Figure 1 depicts the structure of solid-state dye-sensitized solar cells along with a scheme for the electron transfer process. The compact TiO_2 layer is required to prevent direct contact between the transparent conductive oxide (TCO) and hole transporting material (HTM). The fundamental principles of solid-state dye-sensitized solar cells are similar to those of liquid electrolyte based dye-sensitized solar cells except for electron hopping through the HTM layer.

The pores of dye-sensitized mesoporous TiO_2 film should be filled with HTM to induce a heterojunction. A molecular-type HTM, such as 2,2′,7,7′-tetrakis(N,N-p-dimethoxy-phenylamino)-9,9′-spirobifluorene (spiro-MeOTAD), is preferred for pore filling. The hole diffusion length and conductivity in HTM should be considered simultaneously because they limit the thickness of mesoporous TiO_2 film. The TiO_2 film thickness is proportional to the reciprocal of the absorption coefficient, and the higher absorption coefficient is, the thinner TiO_2 film thickness becomes. Because mesoporous TiO_2 film thickness is limited to around 2 μm when using spiro-MeOTAD [13], no significant improvement in solid-state dye-sensitized solar cells is expected from molecular type dyes with absorption coefficients of $\sim 10^3\ cm^{-1}$. This would require a 10-μm-thick TiO_2 film to sufficiently harness the incoming light. To achieve high PCE from solid-state sensitized solar cells, a new light absorber with an absorption coefficient greater than $0.5 \times 10^4\ cm^{-1}$ (=$(2\ \mu m)^{-1}$) is required.

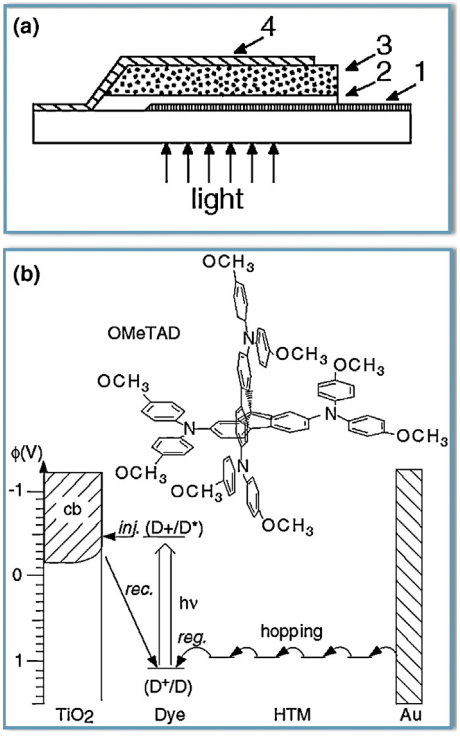

FIGURE 1

(a) Structure of solid-state sensitized solar cell comprised (1) conducting F-doped SnO_2-coated glass, (2) compact TiO_2 layer, (3) dye-sensitized heterojunction (dye-adsorbed TiO_2/hole transporting material) and (4) gold electrode. (b) Scheme for electron-transfer processes that occur in solid-state dye-sensitized heterojunction, where inj., reg. and rec. represent injection, regeneration and recapture, respectively. The chemical structure of spiro-MeOTAD hole transporting material is shown. Reprinted from Ref. [12].

$CH_3NH_3PbX_3$ perovskite light absorber: structure

In perovskite structures with the general formula of ABX_3 (X = oxygen, carbon, nitrogen or halogen), A cation is occupied in a cubo-octahedral site and B cation is occupied in an octahedral site (Fig. 2). When O^{2-} anion is used, A and B are usually divalent and tetravalent, respectively. However, perovskite containing halogen anions allow monovalent and divalent cations in A and B sites, respectively, to fulfill charge neutrality. In $CH_3NH_3PbI_3$, the A-site cation is $CH_3NH_3^+$ and the B-site cation is Pb^{2+}, as shown in Fig. 2b.

The formability of perovskite is estimated based on its geometric tolerance factor (t) [15], $t = (r_A + r_X)/[\sqrt{2}(r_B + r_X)]$, where r_A, r_B and r_X are the effective ionic radii for A, B and X ions, respectively. For transition metal cations containing oxide perovskite, an ideal cubic perovskite is expected when $t = 1$ while octahedral distortion is expected when $t < 1$ [16]. Symmetry also decreases for $t < 1$, which may affect electronic properties [16]. For alkali metal halide perovskite, formability is expected for $0.813 < t < 1.107$ [17]. In Table 1, the r_A in $APbX_3$ (X = Cl, Br, I) perovskite was calculated for $t = 0.8$ and $t = 1$ based on effective ionic radii [18]. A cations with radii between ~1.60 Å and ~2.50 Å were found to form perovskite structures. Thus, methylammonium cation is suitable for lead halide perovskite because its ionic radius is 1.8 Å. Since the tolerance factor of $CH_3NH_3PbI_3$ was calculated as 0.83, deviation from

TABLE 1

Estimation of A cation radii in $APbX_3$

r_{Pb} [a]	X[a]	r_A [b] for $t = 0.8$	r_A [b] (Å) for $t = 1.0$
Pb^{2+} (1.19 Å)	Cl^- (r_{Cl} = 1.81 Å)	1.58 Å	2.43 Å
	Br^- (r_{Br} = 1.96 Å)	1.60 Å	2.50 Å
	I^- (r_I = 2.20 Å)	1.64 Å	2.59 Å

[a] Effective ionic radii for coordination number of 6.
[b] $r_A = t \times [\sqrt{2}(r_B + r_X)] - r_X$.

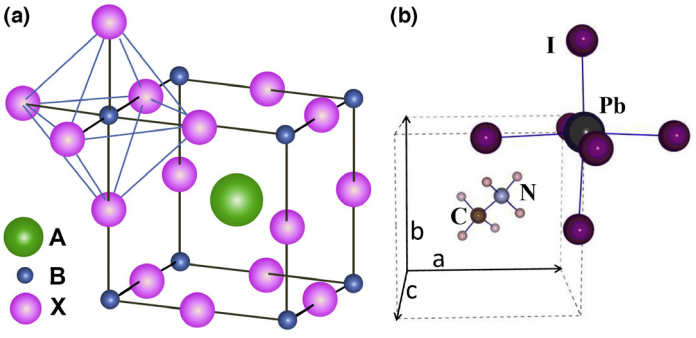

FIGURE 2

(a) ABX_3 perovskite structure showing BX_6 octahedral and larger A cation occupied in cubo-octahedral site. (b) Unit cell of cubic $CH_3NH_3PbI_3$ perovskite. Original figure in (b) was reprinted from Ref. [14].

Please cite this article in press as: N.G. Park, Mater. Today (2014), http://dx.doi.org/10.1016/j.mattod.2014.07.007

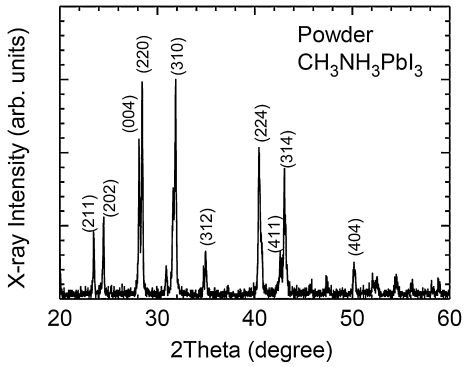

FIGURE 3

X-ray diffraction patterns for $CH_3NH_3PbI_3$ powder, which was prepared by reaction of CH_3NH_3I with PbI_2 in gamma-butyrolactone solution.

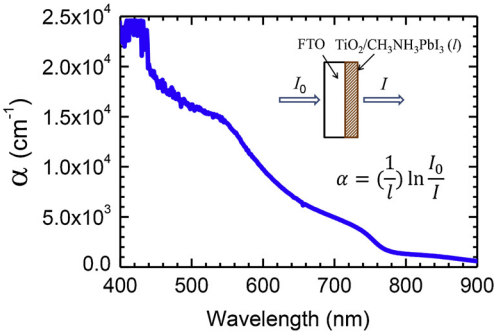

FIGURE 4

Absorption coefficient (α) as a function of wavelength for perovskite $CH_3NH_3PbI_3$ nanodot coated with 1.4 μm TiO_2 film (amount of adsorbed perovskite = $3.2 \times 10^4/\mu m^2$). α was obtained from $T = I/I_0 = \exp(-\alpha l)$, where T, I, I_0 and l represent transmittance, transmitted light intensity, incident light intensity and TiO_2 film thickness, respectively.

an ideal cubic structure is expected. Figure 3 shows the X-ray diffraction pattern of powder $CH_3NH_3PbI_3$ formed from reaction between CH_3NH_3I and PbI_2. The peaks were indexed as a tetragonal phase with lattice parameters of $a = b = 8.883$ Å and $c = 12.677$ Å.

Optical band gap and absorption coefficient of $CH_3NH_3PbX_3$

The absorption coefficient of $CH_3NH_3PbI_3$ was estimated from a nanocrystalline TiO_2 thin film surface coated with $CH_3NH_3PbI_3$. Figure 4 shows the absorption coefficient as a function of wavelength for the $CH_3NH_3PbI_3$ nanodot-coated TiO_2 film. The absorption coefficient was estimated to be 1.5×10^4 cm^{-1} at 550 nm, indicating that the penetration depth for 550 nm light is only 0.66 μm. At 700 nm, the absorption coefficient was 0.5×10^4 cm^{-1}, corresponding to a penetration depth of 2 μm. Most incoming light can be absorbed by the perovskite within a thin layer of about 2 μm, which is suitable as a sensitizer for high efficiency solid-state sensitized solar cells.

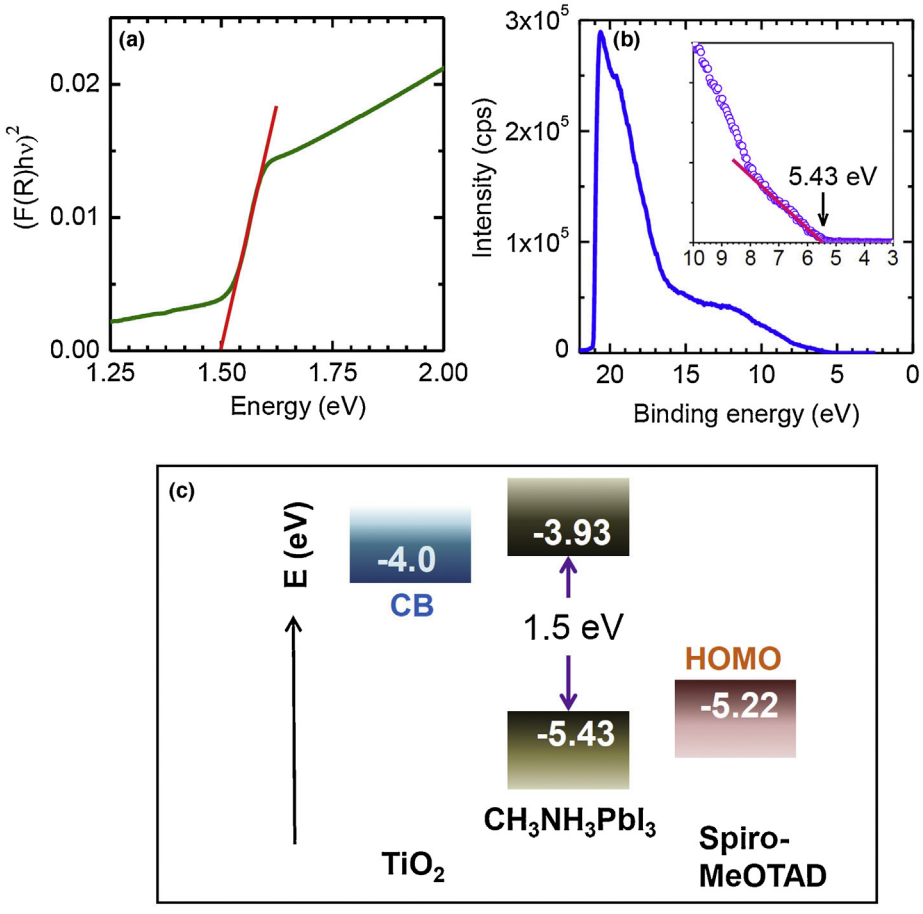

FIGURE 5

(a) Kubelka–Munk plot obtained from diffuse reflectance spectral data and (b) UPS spectrum of $CH_3NH_3PbI_3$-adsorbed TiO_2 film. (c) Schematic energy level diagram of TiO_2, $CH_3NH_3PbI_3$ and spiro-MeOTAD.

Please cite this article in press as: N.G. Park, Mater. Today (2014), http://dx.doi.org/10.1016/j.mattod.2014.07.007

From ultraviolet photoelectron spectroscopy (UPS) and the Tauc plot obtained with UV–vis spectral data, valance band maximum (VBM), band gap, and conduction band minimum (CBM) for $CH_3NH_3PbI_3$ were estimated to be −5.43 eV, −3.93 eV and 1.5 eV, respectively [4], as depicted in Fig. 5. From a thermodynamic viewpoint, the VBM position is suitable for hole separation while CBM is suitable for electron separation. On the basis of band gap energy, the absorption onset wavelength is expected to be around 826 nm.

Balanced charge transport behaviors in $CH_3NH_3PbX_3$

The charge transport properties of $CH_3NH_3PbX_3$ (X = I or $I_{1-x/3}Cl_{x/3}$) perovskites were reported by Xing et al. [19] and Stranks et al. [20]. Transient spectroscopic studies (Fig. 6) revealed that perovskite light absorbers exhibited balanced electron- and hole-transporting behavior. Using diffusion coefficient D and recombination life time τ_e, where D is estimated from a one-dimensional diffusion model [20], the electron diffusion length for $CH_3NH_3PbI_3$ was estimated as 130 nm while the hole diffusion length was estimated as 100 nm. Longer lengths of ~1069 nm for electron diffusion and ~1213 nm for hole diffusion were extracted for $CH_3NH_3PbI_{3-x}Cl_x$. In addition, photo-induced free charge carriers were confirmed in $CH_3NH_3PbI_{3-x}Cl_x$ perovskite [20], indicating that weakly bound excitons were generated by light illumination. Perovskite also has a charge accumulation property that was identified by impedance measurement [21]. This result indicates the existence of a high density state in $CH_3NH_3PbI_3$ and supports weakly bound excitons that can lead to high open-circuit voltage. Findings such as balanced long-range charge diffusion and charge accumulation suggest that perovskite solar cells are designed differently from conventional dye-sensitized solar cells as well as inorganic *pn* junction solar cells.

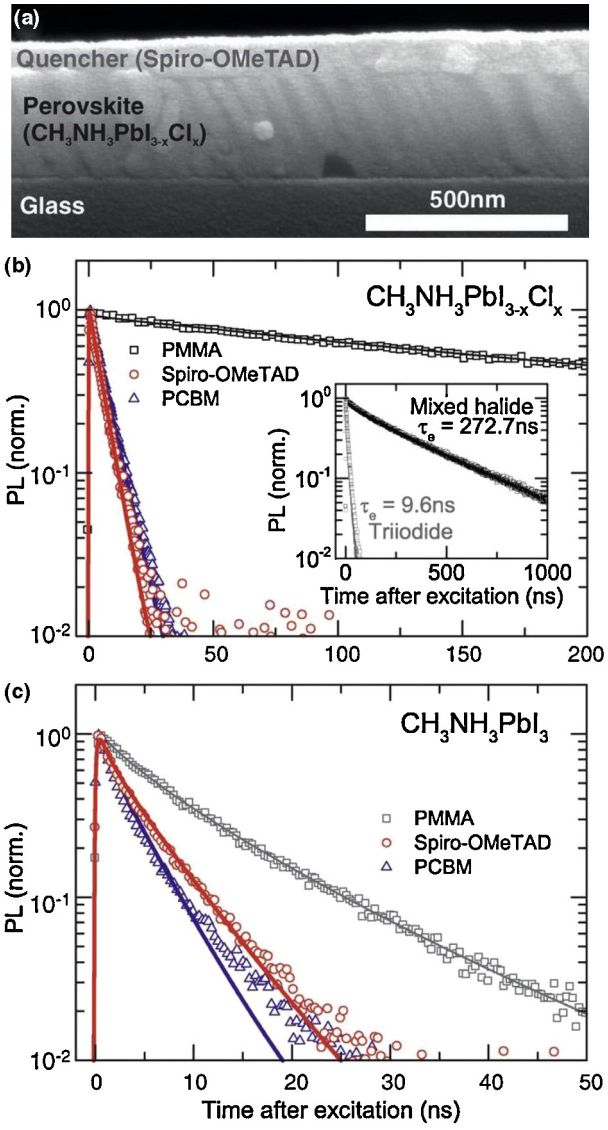

FIGURE 6

(a) Cross-sectional scanning electron microscope (SEM) image of 270-nm-thick mixed halide $CH_3NH_3PbI_{3-x}Cl_x$ absorber layer with hole-quenching layer of spiro-OMeTAD. (b) Photoluminescence (PL) data of one-dimensional diffusion model (described in Ref. [20]) for mixed halide $CH_3NH_3PbI_{3-x}Cl_x$ and (c) 180 nm-thick triiodide $CH_3NH_3PbI_3$ in the presence of electron-quencher PCBM and hole-quencher spiro-MeOTAD without any quenchers (PMMA). (Inset) Comparison of recombination life time of two perovskites (with PMMA). Reprinted from Ref. [20].

Structural evolution of perovskite solar cells

Figure 7 depicts the structural evolution of perovskite solar cells. Perovskite was first used as a sensitizer in dye-sensitized solid-state devices in which molecular dye was replaced by perovskite. In the sensitization concept shown in Fig. 7a, HTM should be fully infiltrated inside the mesoporous oxide layer to induce heterojunction. In addition, oxide layers with electron accepting properties are required to separate the photo-excited electrons in perovskite. Using this sensitization concept, a $CH_3NH_3PbI_3$ nanodot-adsorbed 0.6 μm-thick TiO_2 film demonstrated PCE of 9.7%, photocurrent density (J_{sc}) of 17.6 mA/cm^2, and open-circuit voltage (V_{oc}) of 888 mV [4]. To understand the charge separation in this sensitized structure, a femtosecond transient absorption spectroscopic study was performed with TiO_2 and Al_2O_3. No significant spectral differences between TiO_2 and Al_2O_3 were observed, suggesting that perovskite solar cells may work even without an electron injecting layer.

Perovskite solar cells were confirmed to work in the absence of a mesoporous TiO_2 layer. As shown in Fig. 7b, the $CH_3NH_3PbI_{3-x}Cl_x$ thin layer coated Al_2O_3 film had a PCE of 10.9% [5]. The Al_2O_3 served as a scaffold layer because electron injection from perovskite to Al_2O_3 was not allowed. This result implies that the sensitization concept is not always required for perovskite solar cell design. Moreover, this result suggests that electron transfer can occur in the perovskite layer. A pillared structure was proposed in which the pores of a mesoporous TiO_2 film (pillars) were filled with perovskite instead of a surface coating. As shown in Fig. 7c, a thin capping layer (over layer) was formed after infiltration with the perovskite. With this method, PCE of 12% was reported using $CH_3NH_3PbI_3$ and polytriarylamine (PTAA) [22]. A higher PCE of 15% was achieved from the pillared structure with a two-step coating procedure. In this method, the $CH_3NH_3PbI_3$ layer was prepared by dipping the PbI_2 layer formed in mesoporous TiO_2 film into a diluted CH_3NH_3I solution while the perovskite layer was in contact with spiro-MeOTAD [6]. Since an electron accepting oxide layer is not required, perovskite solar cells can be fabricated from junctions among the perovskite film (intrinsic layer), *n*-type thin TiO_2 film, and *p*-type HTM film. The planar *pin* junction concept, in which 300 nm-thick $CH_3NH_3PbI_{3-x}Cl_x$ film was prepared by co-evaporation of CH_3NH_3I and $PbCl_2$, was confirmed to

Please cite this article in press as: N.G. Park, Mater. Today (2014), http://dx.doi.org/10.1016/j.mattod.2014.07.007

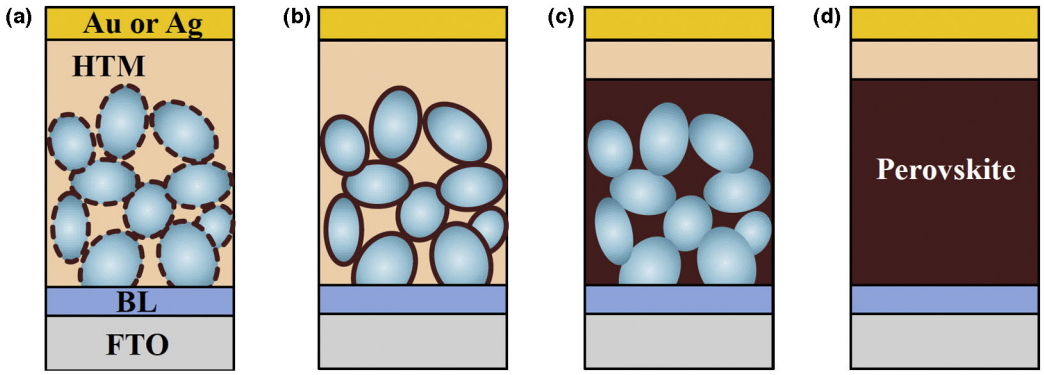

FIGURE 7

Structural evolution of perovskite solar cells: (a) sensitization concept with surface adsorption of nanodot perovskite, (b) meso-superstructure concept with non-injecting scaffold layer, (c) pillared structure with a nano oxide building block, and (d) planar pin heterojunction concept. Spheres represent TiO_2 in (a) and (c) and Al_2O_3 in (b).

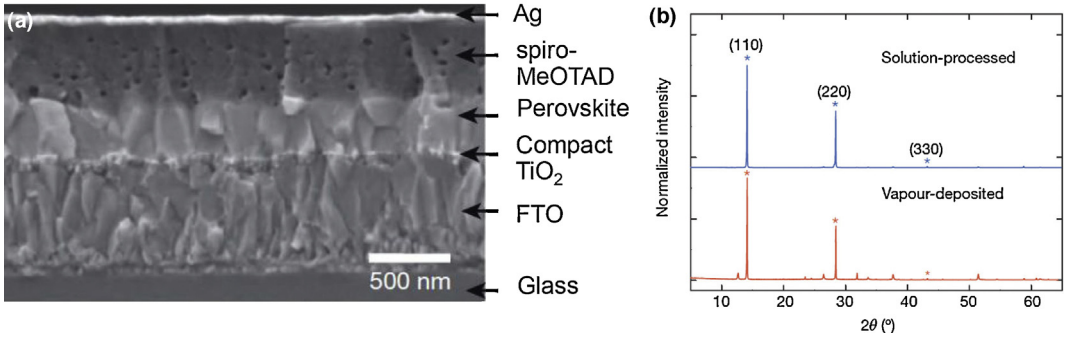

FIGURE 8

(a) Cross-sectional SEM image of planar pin junction structure with vapor-deposited $CH_3NH_3PbI_{3-x}Cl_x$. (b) X-ray diffraction patterns of vapor-deposited and solution-processed $CH_3NH_3PbI_{3-x}Cl_x$. Impurity peaks corresponding to unreacted species are presented in the vapor-deposition process. Reprinted from Ref. [7].

exhibit PCE over 15% [7]. Figure 8 shows a cross-sectional view of the planar structure in which the deposited $CH_3NH_3PbI_{3-x}Cl_x$ film shows only (*h k* 0) peaks in the X-ray diffraction pattern, indicating that Cl^- ions are located in an axial position.

In addition to the sensitization and planar *pin* junction concepts, a *pn* junction structure is available. A *pn* junction structure with FTO/TiO_2/$CH_3NH_3PbI_3$/Au configuration was proposed (Fig. 9) in which $CH_3NH_3PbI_3$ was used as a *p*-type semiconductor [23]. This HTM-free perovskite solar cell initially showed a PCE of 5.5% with a 500 nm-thick nanosheet TiO_2 film for the *n*-type layer. PCE improved to 8% after replacing the TiO_2 nanosheet with a thinner nanoparticle TiO_2 film [24]. A better understanding of the correlation between the depletion region width at the TiO_2–$CH_3NH_3PbI_3$ junction and the PCE led to higher performance approaching 11% [25].

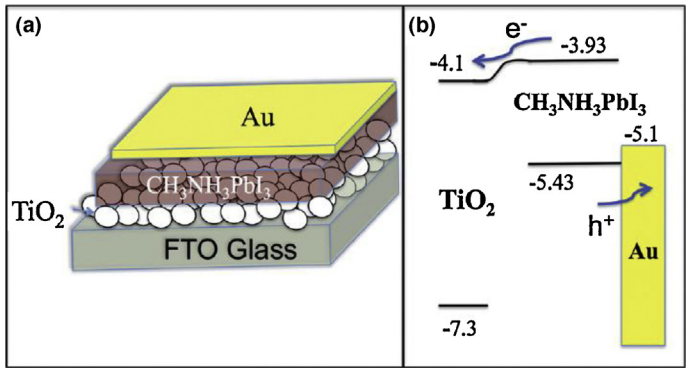

FIGURE 9

(a) Schematic illustration of *pn* junction structure with *p*-type $CH_3NH_3PbI_3$ and n-type TiO_2. (b) Energy level diagram showing the depletion layer between TiO_2 and $CH_3NH_3PbI_3$. Reprinted from Ref. [24].

Stability improvement at high relative humidity

The instability of perovskite at high relative humidity is one issue that needs to be addressed. One method used to solve this problem is the creation of a mixed halide perovskite. The simple solution mixture of $CH_3NH_3PbI_3$ and $CH_3NH_3PbBr_3$ was reported to result in a solid-solution of $CH_3NH_3PbI_{3-x}Br_x$ (x = 0–3) [26]. Since triiodide and tribromide perovskite have a band gap difference, the solid solution resulted in band gap tuning and color control. In addition, the cubic $CH_3NH_3PbI_{3-x}Br_x$ solid-solution perovskite was stable with a humidity soaking test. As shown in Fig. 10, $CH_3NH_3PbI_{2.4}Br_{0.6}$ and $CH_3NH_3PbI_{2.13}Br_{0.87}$ were stable after a humidity soaking test with 55% relative humidity while tetragonal $CH_3NH_3PbI_3$ was unstable. The inclusion of bromide in $CH_3NH_3PbI_3$ will likely enhance the stability of the $CH_3NH_3^+$ cation in the lattice.

Progress in perovskite solar cells

Figure 11 plots the progress in perovskite solar cell efficiency by year. Since 2009, organolead halide perovskites have been used for

Please cite this article in press as: N.G. Park, Mater. Today (2014), http://dx.doi.org/10.1016/j.mattod.2014.07.007

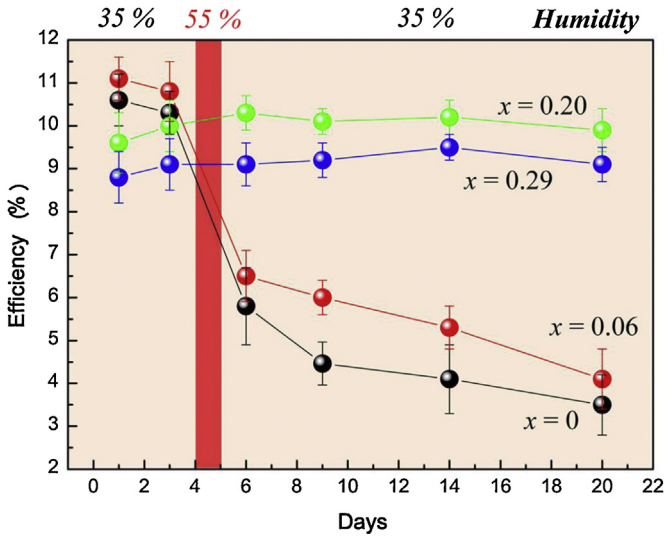

FIGURE 10

Dependence of PCE on relative humidity with time for perovskite solar cell with $CH_3NH_3Pb(I_{1-x}Br_x)_3$ ($x = 0$, 0.06, 0.20, 0.29). Reprinted from Ref. [26].

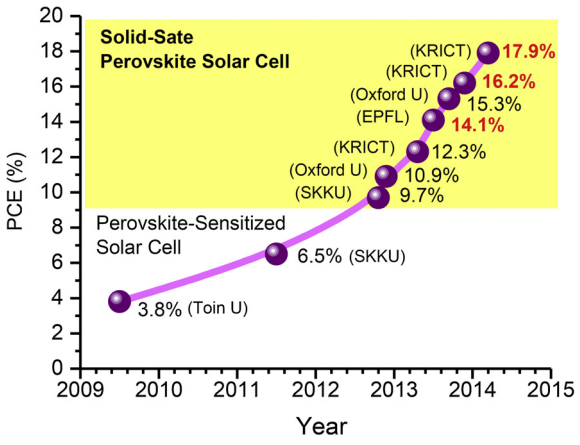

FIGURE 11

Progress in perovskite solar cell efficiency. Perovskite materials have been used since 2009 as sensitizers in dye-sensitized solar cells called perovskite-sensitized solar cells. Solid-state perovskite solar cells, now named as perovskite solar cell, have been developed since 2012. Red PCEs were certified values. SKKU, KRICT and EPFL represent Sungkyunkwan University, Korea Research Institute of Chemical Technology and École polytechnique fédérale de Lausanne, respectively.

solar cells. At first, perovskite light absorbers were used as sensitizers in liquid dye-sensitized solar cells. Perovskite can be dissolved in polar solvent because of its ionic solid nature, which limits further development of perovskite-sensitized photoelectrochemical type solar cells. A long-term stable perovskite solar cell was designed in 2012 by replacing liquid with solid HTM. Since then, solid-state perovskite-containing solar cells have been called perovskite solar cells. As of June 10th 2014, the certified record PCE of 17.9% was achieved by the Korean Research Institute of Chemical Technology (KRICT), which was certified by the National Renewable Energy Laboratory (NREL) [27].

New attempts and better understanding the physicochemical properties of perovskite materials

Except for spiro-MeOTAD as a hole transporting material, inorganic HTMs have been attempted as replacements for organic molecular or polymeric HTMs. NiO showed a promising result in the $TiO_2/CH_3NH_3PbI_3$ heterojunction configuration, where a PCE of 9.5% was achieved with nanocrystalline NiO layer [28]. In this configuration, PCBM and Al were used as electron transporting and collecting layers, respectively. Since the valence band edge of 5.4 eV for NiO is close to that of iodide perovskite (5.3 eV), post-treatment of NiO film using UV light or oxygen plasma is required to improve hole injection efficiency because of an increase in the NiO work function by such post treatments [29]. The electrodeposited NiO layer was confirmed to show an ideal diode behavior [29], however, compared to nanocrystalline NiO [28], the electrodeposited NiO showed a slightly lower PCE of 7.3% due to a lower V_{oc}. UV-ozone post-treated NiO has usually shown a much higher photovoltaic performance than untreated NiO, which is due to not only the change in work function but also an improvement in wettability leading to better chemical interaction between NiO and perovskite [30]. On the basis of the previous reports on CuSCN and CuI as HTMs for the dye-sensitized solid state solar cell [31], those materials were also applied to a perovskite solar cell. Suitable valence band position and high hole conductivity make CuI one of the good candidates for inorganic HTM. CuI deposited from a di-n-propyl sulfide/chlorobenzene mixed solution of CuI showed a PCE of 6% [32]. CuI was found to suffer from the low V_{oc} of less than 0.6 V like CuSCN, which was related to a recombination issue due to free iodine in the CuI layer inducing valence band trap states. The CuSCN film formed on the $CH_3NH_3PbI_{3-x}Cl_x$ by drop-casting from a saturated solution of CuSCN in propylsulfide delivered a PCE of 6.4% [33]. Compared to spiro-MeOTAD, the lower PCE was due to the more than 200 mV lower V_{oc}, which appears to be the main limitation in the CuSCN/perovskite structure. However, the poor performance with CuSCN may not be related to the intrinsic property of CuSCN but to the interfacial problem since $CH_3NH_3PbI_3$ would dissolve while spin-casting the polar CuSCN solution. A better contact between CuSCN and perovskite was realized by modifying two-step deposition of $CH_3NH_3PbI_3$, which demonstrated a PCE of 12.4% with V_{oc} over 1 V [34]. In Fig. 12, the schematic structure and energy diagram for the perovskite solar cell employing a CuSCN HTM are depicted.

It is noted that the charge carrier mobility of the organo metal halide perovskite materials is remarkably high as studied by the combined resistivity and Hall effect data [35]. The electron mobility was estimated to be ~66 cm^2/V s for $CH_3NH_3PbI_3$, ~270 cm^2/V s for $CH_3NH_3Sn_{0.5}Pb_{0.5}I_3$ and ~2320 cm^2/V s for $CH_3NH_3PbSnI_3$, while the hole mobility of the *p*-type $CH_3NH_3SnI_3$ was estimated to be ~322 cm^2/V s. Those charge carrier mobility characteristics of the organo metal halide are almost comparable to inorganic semiconductors such as GaAs. It was confirmed more recently that electron–hole pairs were separated immediately in 2 ps after photoexcitation and the separated charges exhibited mobility as high as 25 cm^2/V s together with microsecond long-lived characteristics [36]. It was also mentioned that a metal oxide with high electron mobility might improve photovoltaic performance of the $CH_3NH_3PbI_3$ perovskite solar cell since electron injection to TiO_2 led to unbalanced charge transport [37]. Regarding charge diffusion length, the diffusion length is critical in designing the perovskite layer thickness and structure. Early investigation on $CH_3NH_3PbI_3$ and

Please cite this article in press as: N.G. Park, Mater. Today (2014), http://dx.doi.org/10.1016/j.mattod.2014.07.007

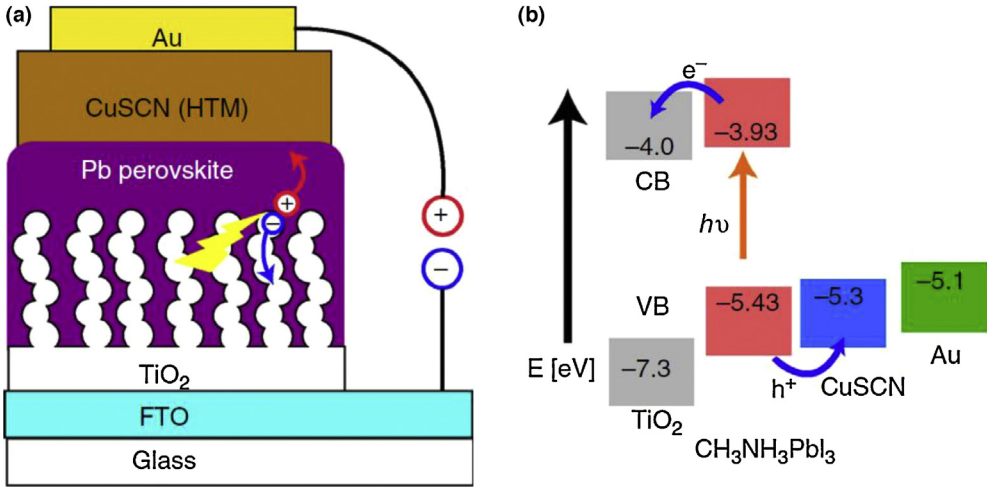

FIGURE 12

(a) Schematic structure and (b) energy diagram for the $CH_3NH_3PbI_3$ perovskite solar cell based on inorganic CuSCN HTM. Reprinted from Ref. [34].

$CH_3NH_3PbI_{3-x}Cl_x$ showed that the balanced charge carrier diffusion length was estimated to be ~100 nm for triiodide and ~1000 nm for mixed iodide [19,20]. Longer charge carrier diffusion length was estimated to be ~1900 nm for electrons and ~1500 nm for holes in $CH_3NH_3PbI_{3-x}Cl_x$ from the electron beam induced current (EBIC) study [37]. Such a discrepancy in carrier diffusion length is likely to be attributed to the perovskite layer morphology, which suggests that the perovskite layer morphology is critical in terms of charge carrier diffusion behavior. Those estimated charge carrier diffusion lengths were based on the planar structures without employing a mesoporous TiO_2 layer. The longer electron diffusion length up to 1.5 μm was evaluated for the $CH_3NH_3PbI_3$ perovskite solar cell with the 650 nm-thick mesoporous TiO_2 layer [38], which indicates that the submicrometer TiO_2 layer hardly limits the photocurrent in perovskite solar cells.

Future direction and challenges

Recent progress in perovskite solar cells based on organolead halides has been reviewed here. $CH_3NH_3PbI_3$ and mixed halide perovskite $CH_3NH_3PbI_{3-x}Cl_x$ are at the center of research into high efficiency perovskite solar cells. With these materials, a PCE of 20% is expected from single junction structures and a PCE of 29% is expected from tandem structures [39,40]. Higher efficiency is still possible through structural modification [40], along with band gap tuning. Modification of the bond distance and/or angle of X–Pb–X in $CH_3NH_3PbX_3$ is one of strategies to tune band gap energy. More recently, a PCE approaching 30% was achieved from a single junction perovskite solar cell [41]. Optimistic expectations for the perovskite solar cell are based on the superb opto-electronic property of organo metal halide perovskite material that is even better than high efficiency GaAs. Since the high V_{oc} observed from organo metal halide perovskite is likely to be related to high internal photoluminescence quantum efficiency [42], careful control of the luminescent property of perovskite could further improve V_{oc}, hence contributing to an even higher PCE. For commercialization, environmental and photo-stabilities should be guaranteed. For this to be achieved, encapsulation technology and materials with humidity-resistance and photo-stability must be developed. Scale-up technologies for high efficiency module fabrication are also an important challenge. Finally, substitution of other elements for Pb [43,44] is one of the important tasks for environmentally friendly perovskite solar cells.

Acknowledgements

This work was supported by National Research Foundation of Korea (NRF) grants funded by the Ministry of Science, ICT, & Future Planning (MSIP) of Korea under contracts No. NRF-2010-0014992, NRF-2012M1A2A2671721, 2012M3A7B4049986 (Nano Material Technology Development Program) and NRF-2012M3A6A7054861 (Global Frontier R&D Program on Center for Multiscale Energy System).

References

[1] D.B. Mitzi, et al. Nature 369 (1994) 467–469.
[2] A. Kojima, et al. J. Am. Chem. Soc. 131 (2009) 6050–6051.
[3] J.-H. Im, et al. Nanoscale 3 (2011) 4088–4093.
[4] H.-S. Kim, et al. Sci. Rep. 2 (2012) 591.
[5] M.M. Lee, et al. Science 338 (2012) 643–647.
[6] J. Burschka, et al. Nature 499 (2013) 316–319.
[7] M. Liu, M.B. Johnston, H.J. Snaith, Nature 501 (2013) 395–398.
[8] Science News, Science 342 (2013) 1438–1439.
[9] Nature News Features, Nature 504 (2013) 357–365.
[10] B. O'Regan, M. Grätzel, Nature 353 (1991) 737–740.
[11] A. Yella, et al. Science 334 (2011) 629–634.
[12] U. Bach, et al. Nature 395 (1998) 583–585.
[13] H.-S. Kim, et al. Bull. Korean Chem. Soc. 33 (2012) 670–674.
[14] G. Giorgi, et al. J. Phys. Chem. Lett. 4 (2013) 4213–4216.
[15] V.M. Goldschmidt, Ber. Dtsch. Chem. Ges. 60 (1927) 1263–1268.
[16] M. Rini, et al. Nature 449 (2007) 72–74.
[17] C. Li, et al. Acta Crystallogr. B 64 (2008) 702–707.
[18] R.D. Shannon, Acta Crystallogr. A 32 (1976) 751–767.
[19] G. Xing, et al. Science 342 (2013) 344–347.
[20] S.D. Stranks, et al. Science 342 (2013) 341–344.
[21] H.-S. Kim, et al. Nat. Commun. 4 (2013) 2242.
[22] J.H. Heo, et al. Nat. Photonics 7 (2013) 486–491.
[23] L. Etgar, et al. J. Am. Chem. Soc. 134 (2012) 17396–17399.
[24] W.A. Laban, L. Etgar, Energy Environ. Sci. 6 (2013) 3249–3253.
[25] S. Aharon, et al. Phys. Chem. Chem. Phys. 16 (2014) 10512–10518.
[26] J.H. Noh, et al. Nano Lett. 13 (2013) 1764–1769.
[27] Research Cell Efficiency Records, NREL. http://www.nrel.gov/ncpv/.
[28] K.-C. Wang, et al. Sci. Rep. 4 (2014) 4756.
[29] A.S. Subbiah, et al. J. Phys. Chem. Lett. 5 (2014) 1748–1750.

Please cite this article in press as: N.G. Park, Mater. Today (2014), http://dx.doi.org/10.1016/j.mattod.2014.07.007

[30] J.-Y. Jeng, et al. Adv. Mater. (2014), http://dx.doi.org/10.1002/adma.201306217.
[31] H.J. Snaith, L. Schmidt-Mende, Adv. Mater. 19 (2007) 3187–3190.
[32] J.A. Christians, R.C.M. Fung, P.V. Kamat, J. Am. Chem. Soc. 136 (2014) 758–764.
[33] S. Chavhan, et al. J. Mater. Chem. A (2014), http://dx.doi.org/10.1039/x0xx00000x.
[34] P. Qin, et al. Nat. Commun. 5 (2014) 3834.
[35] C.C. Stoumpos, C.D. Malliakas, M.G. Kanatzidis, Inorg. Chem. 52 (2013) 9019–9020.
[36] C.S. Ponseca Jr., et al. J. Am. Chem. Soc. 136 (2014) 5189–5190.
[37] E. Edri, et al. Nat. Commun. 5 (2014) 3461.
[38] Y. Zhao, A.M. Nardes, K. Zhu, J. Phys. Chem. Lett. 5 (2014) 490–494.
[39] N.-G. Park, J. Phys. Chem. Lett. 4 (2013) 2423–2430.
[40] H.J. Snaith, J. Phys. Chem. Lett. 4 (2013) 3623–3630.
[41] W.-J. Yin, T. Shi, Y. Yan, Adv. Mater. (2014), http://dx.doi.org/10.1002/adma.201306281.
[42] P.K. Nayak, D. Cahen, Adv. Mater. (2014), http://dx.doi.org/10.1002/adma.201304620.
[43] Y. Ogomi, et al. J. Phys. Chem. Lett. 5 (2014) 1004–1010.
[44] N.K. Noel, et al. Energy Environ. Sci. (2014), http://dx.doi.org/10.1039/x0xx00000x.

Please cite this article in press as: N.G. Park, Mater. Today (2014), http://dx.doi.org/10.1016/j.mattod.2014.07.007